Hindawi Publishing Corporation
Journal of Nanomaterials
Volume 2013, Article ID 627385, 11 pages
http://dx.doi.org/10.1155/2013/627385

Research Article

Solvothermal Synthesis of TiO_2 Photocatalysts in Ketone Solvents with Low Boiling Points

Chau Thanh Nam,[1] Wein-Duo Yang,[1,2] and Le Minh Duc[3]

[1] *Department of Chemical and Materials Engineering, National Kaohsiung University of Applied Sciences, 415 Chien-Kung Road, Kaohsiung 807, Taiwan*
[2] *Department of Chemical and Biotechnology Engineering, University of Colorado at Boulder, Boulder, CO 80309, USA*
[3] *Department of Chemical Engineering, Da Nang University of Technology, Da Nang, Vietnam*

Correspondence should be addressed to Wein-Duo Yang; ywd@cc.kuas.edu.tw

Received 4 February 2013; Revised 13 April 2013; Accepted 18 April 2013

Academic Editor: Yanbao Zhao

The titanium dioxide (TiO_2) photocatalysts were synthesized by a solvothermal process in highly alkaline 70 : 30 water : ketone solutions with a TiO_2-P25 precursor and calcined at different temperatures. The ketone solvents, such as acetone and methyl ethyl ketone (MEK), had low boiling points (<100°C). The as-prepared samples were characterized by XRD, TEM, FTIR, UV-vis and Raman spectroscopy. The effects of the different solvents on the nanostructure, the morphology, and the photocatalytic performance of the TiO_2 products were investigated. Nanotubes formed in water and water-MEK, while nanoparticle/nanowires formed in water-acetone and water-acetone-MEK. The ketone solvents played an important role in the improving nanostructure properties of these products, which affected their photocatalytic reactions. The results indicated that samples synthesized in solvents such as water and MEK had high adsorption and photocatalytic behaviors. The photocatalytic reactivity was the greatest for the TiO_2 prepared in MEK and calcined at 100°C, which was even more reactive than the sample prepared in water and TiO_2-P25 powder.

1. Introduction

Titanium dioxide (TiO_2) is a common metaloxide semiconductor that is used in many key industrial applications, such as in the construction of photocatalysts, solar cells, microelectronics, and electrochemical devices. Many researchers have focused on applications of TiO_2 in photocatalytic materials due to of its low cost, nontoxicity, chemical stability, oxidizing strength, and powerful photocatalytic activity [1, 2]. Many methods of synthesizing TiO_2 nanotubes, including wet chemical techniques, such as sol-gel, precipitation, and hydrothermal/solvothermal, have been applied successfully to synthesize different TiO_2 nanostructures [3–8]. Currently, liquid-phase processing at low temperatures is an effective synthetic route for producing TiO_2 nanostructures [9–16] and hydrothermal/solvothermal techniques are used widely to synthesize TiO_2 nanostructures [17–24]. Hydrothermal/solvothermal syntheses are advantageous given that they facilitate the synthesis of nanometer-sized crystalline TiO_2 powders at relatively low temperatures [20, 22, 23]. Solvothermal reactions, which use a solvent under conditions of high pressure and mild temperature, show promise for developing nanotechnologies [25]. The use of organic solvents in solvothermal synthesis helps to control the structure and morphology of the products due to their shape- and size-dependent properties [22, 23, 26]. The addition of an organic solvent to water provides an excellent reaction medium for the hydrothermal processing of nanoparticles given that these mixtures modulate the reaction rate and equilibrium by adjusting the dielectric constant and the density of the solvent with respect to pressure and temperature thus producing faster reaction rates and smaller particles [27]. Alcohol, which is utilized often as an organic solvent, is believed to play an important role in

the formation of titania phases [23]. A number of different solvents were used in solvothermal syntheses to investigate the growth mechanisms and characteristics of titania [22, 26]. In previous studies, ketones were rarely used as solvents in the syntheses but were used (mainly acetone) in postsynthesis washing processes [17, 19, 28–30]. Therefore, the effects of ketone solvents, especially solvents with low boiling points such as acetone (Ac) and methyl ethyl ketone (MEK), on the structures, morphologie, and optical properties of TiO_2 are unknown.

The photocatalytic behavior of titania depends significantly on its microstructure and preparation method [31]. However, the size, the morphology, and the structural properties of TiO_2 nanostructures depend on the TiO_2 precursors and reaction parameters, such as the reaction temperature, the reaction time, and the solution pH during the reaction [32, 33]. In this study, we synthesized TiO_2 nanostructures by solvothermal routes (at 130°C, for 24 h) in highly alkaline solutions using ketone solvents with low boiling points (acetone and methyl ethyl ketone) and TiO_2-P25 nanoparticles as precursors and calcined the products at different temperatures. We investigated the effects of different solvents on the nanostructure, the phase composition, the morphology, the pore volume and size, and the specific surface area of the products, as well as the efficiency of the photocatalytic reactions associated with the degradation of a dye (methylene blue). This solvothermal method shows promise as an efficient, energy-saving strategy because synthesis and calcination are performed at low temperatures. Moreover, the products are highly efficient photocatalysts as demonstrated by their ability to decolor organic dyes under visible-light irradiation.

2. Materials and Methods

2.1. Reagents. Analytical grade chemicals were used as received without any further purification. NaOH, TiO_2 (P25) powder, and methylene blue (MB) were purchased from Across Organics (NJ, USA). A 200 mL solution of MB (300 ppm) was prepared in double-distilled water and diluted as required.

2.2. Instrumentation. Glassware was washed thoroughly in tap water, followed by distilled water; it was then dried overnight in a hot-air oven at 50°C. The crystal structures of the products were characterized by X-ray diffraction (PANalytical, X Pert PRO X-ray diffractometer, CuK_α radiation) and micro-Raman spectroscopy (Dimension-P2 Raman). A Micromeritics ASAP 2020 analyzer was used for BET analysis. TEM measurements were performed using a Philips, M-200 transmission electron microscope operated at 200 kV. Samples for TEM analysis were prepared by sonicating products in ethanol for 15 min, depositing 2-3 drops on thin carbon films supported on a copper grids, and drying overnight at 60°C. A Fourier transform infrared spectroscopy (FTIR) study was conducted with a PerkinElmer spectrophotometer. A Jasco V-600 UV-vis spectrophotometer was used to record diffused UV-vis reflectance spectra in the 300–800 nm range and to measure red shifts. Absorbance measurements were carried out using a UV-Vis spectrophotometer (Hitachi, U-2800) equipped with a 1 cm quartz cell.

2.3. Preparation TiO_2 Nanostructures. Solutions of 10 M NaOH were prepared by adding 28 g NaOH to 70 mL of a 70 : 30 mixed solvent of distilled water and ketones. The ketone solvents had low boiling points, less than the boiling point of water (100°C), such as acetone (Ac) and methyl ethyl ketone (MEK). The samples were named as shown in Table 1. In a typical procedure, 2.1 g TiO_2-P25 powder was added to 70 mL of 10 M NaOH in a 70 : 30 mixture of water and ketone solvent and stirred continuously for 30 min with a magnetic stirrer. Then, the mixture was sonicated for 30 min. Next, this homogeneous suspension was hydrothermally treated in a stainless steel, Teflon-lined autoclave at 130°C for 24 h. Afterwards, the reactor cooled naturally in air to room temperature. The reaction products were washed thoroughly with large volumes of double-distilled water to achieve a neutral pH (≈7). The solids were collected by filtration and dried at 80°C for 6 h. The products were calcined at different temperatures for 2 h to obtain TiO_2 nanostructures. Lastly, the products were used to remove MB by photocatalytic degradation under visible-light irradiation. To study the effects of the ketone cosolvents on the morphologies and properties of TiO_2 structures, we used a 1 : 1 acetone : MEK solvent in a 70 : 30 water : solvent mixture. After mixing with NaOH, the pH values of the 70 : 30 water : ketone solvents were 9.96 (acetone), 10.28 (MEK), and 10.36 (A : MEK = 1 : 1).

2.4. Photocatalytic Degradation of Aqueous Methylene Blue (MB). Photocatalytic degradation experiments were carried out by dispersing 0.01 g TiO_2 nanostructures in 100 mL MB solution with an initial dye concentration (C) of 21 mg/L (dose of 0.1 g/L) and stirring for 1 h in darkness. Suspensions of dyes and catalysts were added to a photocatalytic reaction vessel under visible-light irradiation. A 300 W halogen lamp with a 410 nm cut-off glass filter was used as the light source. These photocatalytic degradation measurements were conducted at room temperature (≈25 ± 2°C) and atmospheric pressure. The reaction temperature was controlled by continuously circulating cool water outside of the vessel during the irradiation process. The total duration of visible-light irradiation was 2 h. Every 15 min, approximately 8 mL of solution was removed and immediately centrifuged at 4000 rpm for 10 min. The MB dye concentration remaining in the solution was measured with a UV-Vis spectrophotometer at the maximum absorption wavelength of 664 nm. The blue color of the solution gradually faded over time because MB was adsorbed on TiO_2 particles and was degraded by light.

3. Results and Discussion

3.1. Characterization of TiO_2 Nanostructures. The crystal structure, morphology, and size of the synthesized products were determined using XRD and TEM (Table 2). The MEK sample of TiO_2 (prepared using methyl ethyl ketone) and TiO_2 samples (prepared in different solvents) with the best

Table 1: The effects of various solvents on specific surface areas (S_{BET}) and pore parameters.

Sample	Solvent	Calcination temperature, °C	S_{BET}, m^2/g	Pore volume, cm^3/g	Pore size, nm
W100	Water	100	213.4	0.370	6.2
A100	Acetone	100	48.7	0.244	18.2
AMEK200	Acetone : methyl ethyl ketone (1 : 1)	200	78.7	0.274	13.2
MEK100	Methyl ethyl ketone	100	200.8	0.277	5.5
MEK200	Methyl ethyl ketone	200	183.6	0.266	5.9
MEK300	Methyl ethyl ketone	300	171.1	0.306	6.4
MEK400	Methyl ethyl ketone	400	130.1	0.313	8.8
MEK500	Methyl ethyl ketone	500	34.3	0.288	33.5

Table 2: The effect of different solvents on morphologies, sizes and structures of TiO_2 nanostructures.

Sample	Composition, %	Morphology	Size, nm	Band gap, eV	FWHMs, °	Titanate crystallite size, nm
W100	Titanate (100)	Nanotube	6-7	3.20	0.651	12.3
A100	Titanate (100)	Nanowire, nanoparticle	50 (nanoparticle)	3.36	0.784	10.2
AMEK200	Titanate (100)	Nanotube, nanowire, and nanoparticle	6-7 (nanotube)	3.45	0.515	15.6
MEK100	Titanate (100)	Nanotube	6-7	3.21	0.862	9.3
MEK200	Titanate (100)	—	—	3.22	0.787	10.2
MEK300	Titanate (100)	—	—	3.20	0.764	10.5
MEK400	Titanate (100)	—	—	3.22	0.746	10.8
MEK500	Titanate (63.9), anatase (19.1), and rutile (17)	—	—	3.29	0.281	28.6
TiO_2 precursor	Anatase (81), rutile (19)	Nanoparticle	25	3.25	—	—

photocatalytic performance were compared to samples synthesized in water and the TiO_2-P25 precursor.

The XRD patterns of various samples are shown in Figure 1. The samples prepared using MEK and calcined at temperatures up to 400°C exhibited mainly diffraction lines of titanate phases, Figure 1(a); these results are similar to those of previous work [34]. However, when the sample was heated at 500°C, the diffraction pattern corresponded to a mixture of anatase (48°), rutile (44.6°), and sodium trititanate phases (28.9, 29.8, 33.1, and 67.1°). This XRD analysis was consistent with the phase composition that was determined quantitatively with the normalized RIR method, summarized in Table 2. Similar results reported by Zárate et al. [35] indicated that a sample synthesized in 10 M NaOH during 18 h was stable when heated up to 400°C and was transformed into sodium hexatitanate when calcined at 500°C. This transformation of TiO_2 into sodium trititanate showed that it was not possible to completely eliminate sodium from the samples, and after a long period of hydrothermal treatment, Na^+ formed in the structure of the calcined samples [35]. The sample prepared using MEK was thermally stable up to 400°C, and the relative intensity of the peaks of the titanate phases underwent very little change although peak intensities increased significantly after calcination at 500°C. The average crystal size (d), determined by applying the Scherrer equation [36] and using the full width at half maximum (FWHM) of the titanate phases, are given in Table 2: $d = 0.9\lambda/B\cos\theta$, where λ is the X-ray wavelength (0.15418 nm), θ is the Bragg angle, and B is the FWHM. These results show that the FWHM of the peaks decreased gradually when the calcination temperature increased, especially at 500°C, at which the FWHM decreased significantly, an effect that may be attributed to increased crystallinity. However, calcination at 500°C resulted in the growth of nanocrystals up to 28.6 nm, and this size increase is significant compared to the MEK100 (9.3 nm) sample that was calcined at a low temperature. Figure 1(b) shows that all of the samples contained peaks corresponding to titanate phases. The FWHM of the peaks decreased in the following order: MEK100 < A100 < W100 < AMEK200. This order suggested that, when products were calcined at the same temperature, smaller crystals formed when ketone solvents (acetone, MEK) were used than when water alone was used as the solvent (see results in Table 2).

The phase components of the samples were characterized by Raman spectroscopy, Figure 2. The spectrum for the sample of TiO_2-P25 precursor exhibited the characteristics of anatase phase scattering at approximately 144, 399, 515, and 638 cm^{-1} [37–40]. Raman spectra of the rutile phase

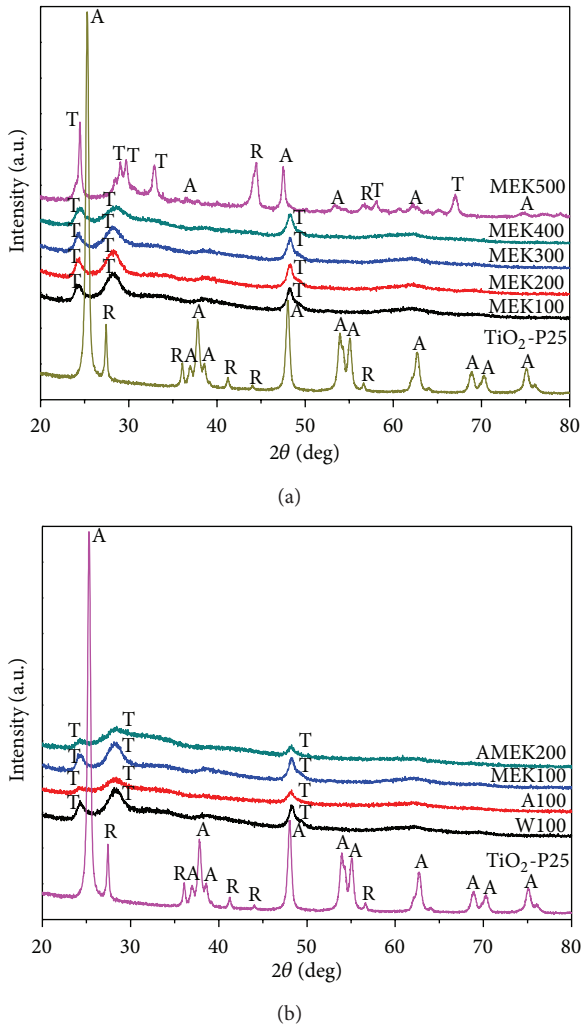

Figure 1: XRD patterns. (a) Samples prepared using MEK and calcined at different temperatures, and (b) samples using various solvents and calcined at different temperatures. The notations T, A, and R correspond to titanate, anatase, and rutile, respectively. The reference patterns correspond to the JCPDS: number 21-1272 (anatase), number 21-1276 (rutile), number 31-1329 (sodium trititanate), and number 47–561 (hydrogen trititanate).

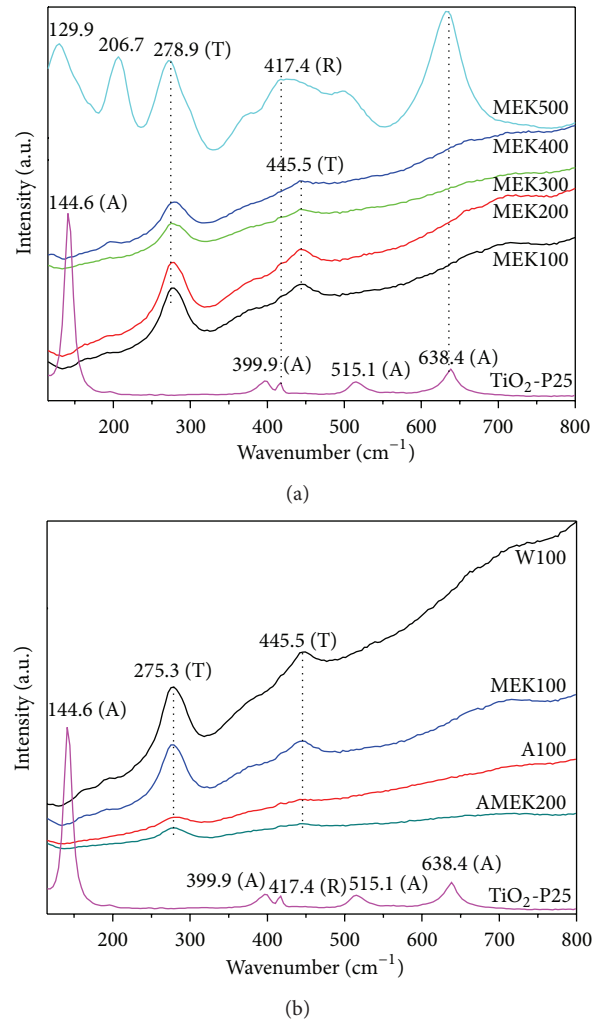

Figure 2: Raman spectra. (a) Samples prepared using MEK and calcined at different temperatures, and (b) samples prepared using various solvents and calcined at different temperatures. The notations T, A, and R correspond to titanate, anatase, and rutile, respectively.

were rarely reported to contain a medium intensity peak at approximately 417 cm^{-1} [41]. However, to be compatible with the results of XRD patterns in Figure 1, this peak should be assigned to the rutile phase because the TiO_2-P25 precursor included a mixture of anatase and rutile phases. The titanate nanotubes produced a unique spectrum with moderate to strong intensity bands at 445, 275, and 278 cm^{-1} [34, 35, 40]. Raman investigations complemented the XRD analysis, showing that titanate phases existed for the samples prepared using MEK and calcined at temperatures from 100 to 400°C. At 500°C, the Raman spectrum contained peaks for the anatase (638.4 cm^{-1}) and rutile (417 cm^{-1}) phases as well as some new peaks at 129.9 and 206.7 cm^{-1} (Figure 2(a)). These new peaks may belong to titanate phases (forms of sodium trititanate), and they are fully consistent with the XRD analysis of the sample prepared using MEK and calcined at 500°C. The thermal stability of these samples can be considered from Raman spectra and XRD patterns. Up to 400°C, the samples still exhibited the titanate phase characteristic of the as-synthesized samples. At 500°C, the sample began to partially transform to the anatase (peaks at 48° in the XRD and at 638.4 cm^{-1} in the Raman results) and the rutile (peaks at 44.6° in the XRD and at 417 cm^{-1} in the Raman results) phases. New peaks corresponding to sodium titanate also appeared (peaks at 28.9, 29.8, 33.1, and 67.1° in the XRD patterns and at 129.9 and 206.7 cm^{-1} in the Raman spectra). These results partially resembled results from previous studies [34, 35]. Similar to the XRD analysis, Figure 2(b) showed that all peaks corresponding to the titanate phase (at 275.3 and 445.5 cm^{-1}) were more intense and clearer for the W100 and MEK100 samples than the A100 and AMEK200 samples.

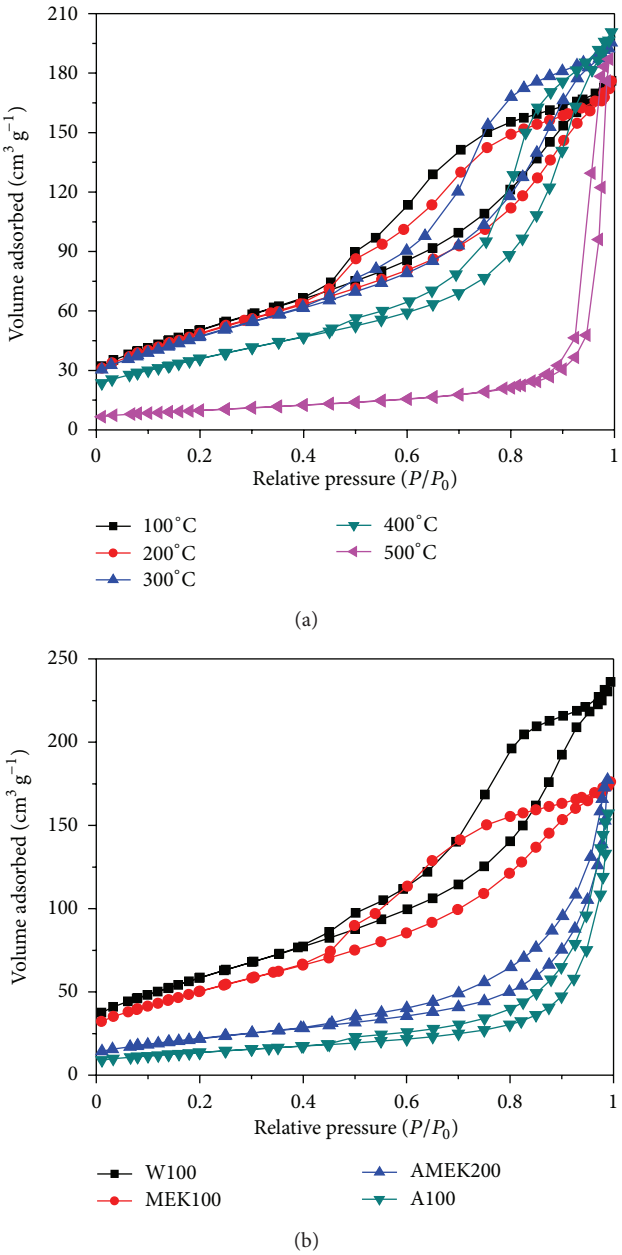

Figure 3: Nitrogen adsorption-desorption isotherms. (a) Samples prepared using MEK and calcined at the different temperatures, and (b) samples prepared using various solvents and calcined at different temperatures.

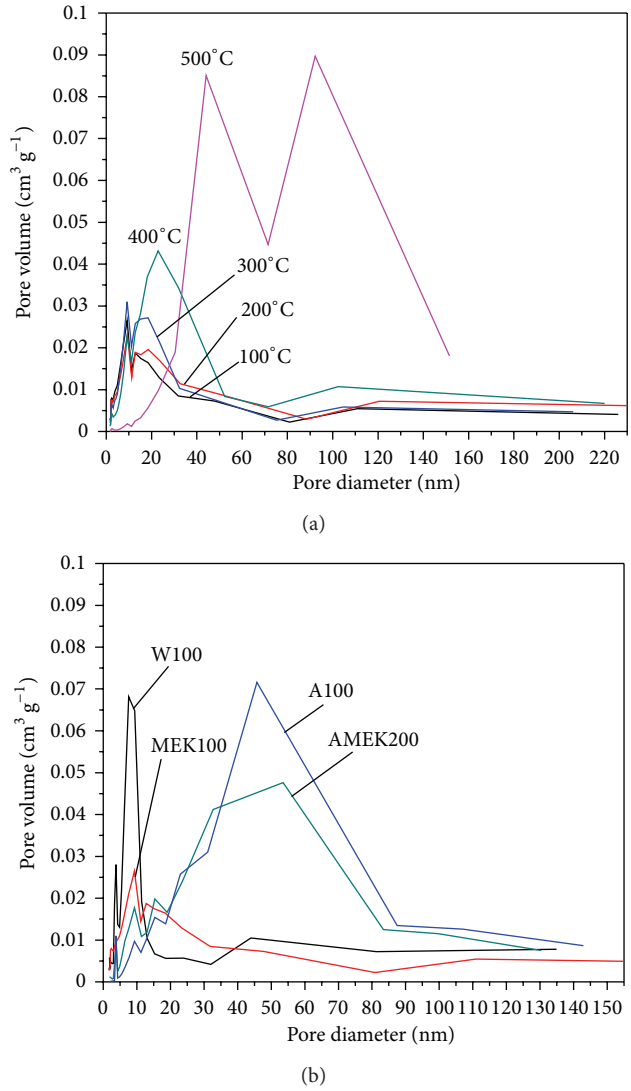

Figure 4: Pore distribution. (a) Samples prepared using MEK and calcined at different temperatures, and (b) samples prepared using various solvents and calcined at different temperatures.

The nitrogen adsorption-desorption isotherms of samples prepared using MEK and various solvents and calcined at different temperatures are presented in Figure 3. Specific surface areas (S_{BET}), average pore volumes, and pore sizes of these samples are summarized in Table 1.

According to the BDDT classification system, the isotherms of samples W100, MEK100, MEK200, MEK300, and MEK400 were type IV with type H2 and type H3 hysteresis loops, and the isotherms of samples MEK500, A100, and AMEK200 were type II with type H3 hysteresis loops [42].

Generally, the W100 and MEK samples that were calcined from 100 to 400°C exhibited high specific surface areas (S_{BET}). As shown in Figure 3, the capillary cohesion of the MEK500 (Figure 3(a)) and A100 (Figure 3(b)) samples occurred at the highest pressure, suggesting that these samples had the largest pore sizes and the smallest specific surface areas (Table 1). For the sample prepared using MEK, S_{BET} decreased gradually as the calcination temperature increased. The hysteresis loops shifted to higher relative pressures, indicating that the pore size grew gradually because TiO_2 crystal growth leads to the formation of larger pores. The samples had high S_{BET} values and pore volumes, which greatly improved adsorption efficiency. It is remarkable that the specific surface area was higher for the products than for the TiO_2-P25 precursor.

Figure 4 shows pore size distributions, which were relatively narrow for samples prepared in MEK and calcined

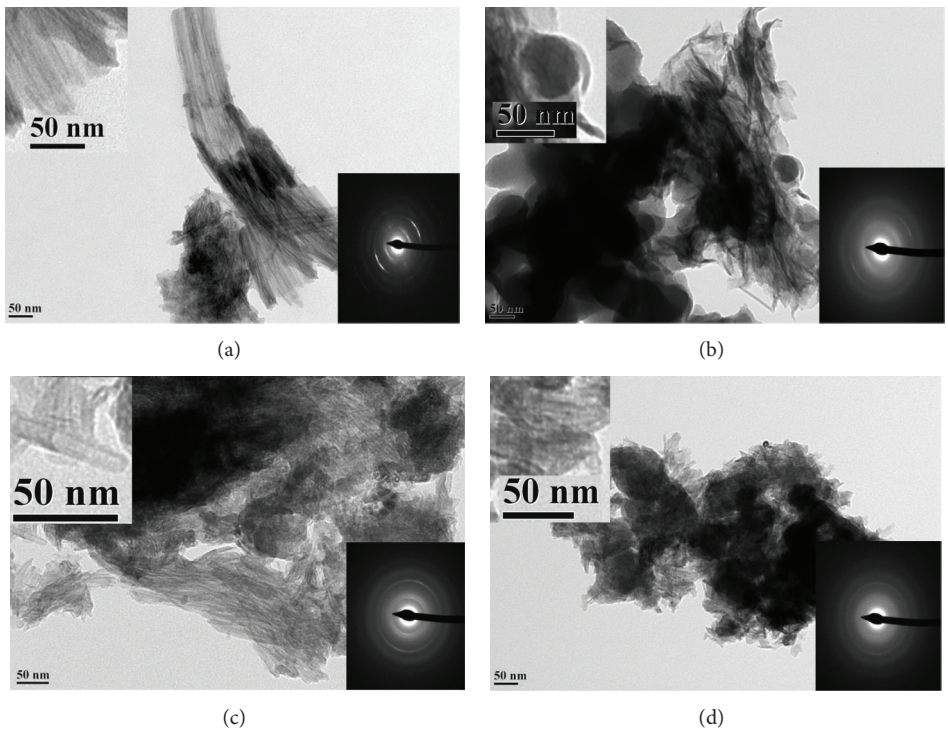

Figure 5: TEM images of samples prepared using various solvents and calcined at different temperatures. (a) W100, (b) A100, (c) MEK100, and (d) AMEK200.

at temperatures from 100 to 300°C (Figure 4(a)) and sample W100 (Figure 4(b)). The sizes were somewhat wider for sample MEK400 and the widest for sample MEK500 (Figure 4(a)). Similarly, samples A100 and AMEK200 (Figure 4(b)) exhibited a wider pore size distribution (5–90 nm) than samples W100 and MEK100 (3–15 nm).

Figure 5 shows TEM images of samples with the highest photocatalytic efficiency for each of the different solvents. The insets show the corresponding selected area electron diffraction (SAED) patterns and the sample dimensions. These SAED patterns show that the as-prepared samples contain crystallites in polycrystalline phases. In addition, samples W100 (Figure 5(a)) and MEK100 (Figure 5(c)) exhibited predominantly tube-like structures, sample A100 (Figure 5(b)) showed both nanoparticle and nanowire structures, and sample AMEK200 (Figure 5(d)) contained a combination of nanoparticles, nanowires, and a small amount of nanotubes. The nanotubes in these samples exhibited an outside diameter of approximately 6-7 nm and lengths of several hundred nanometers. The ends of these nanotubes were open, which was extremely beneficial for adsorption and photocatalysis. The left inset in Figure 5 is an enlarged picture of these samples. Sample A100 (Figure 5(b)) showed nanoparticles with an average diameter of ca. 50 nm. These TEM images are very beneficial for interpreting the effectiveness of photocatalytic reactions that are presented in detail in a later section. In particular, the use of water and MEK in aqueous NaOH solutions promoted the formation of nanotubes, revealing that the ketone solvent MEK positively affected the solvothermal synthesis of TiO_2 nanotubes.

Figure 6 shows FTIR spectra of samples that were prepared using different solvents and that showed the highest photocatalytic efficiency. As shown in Figure 6, all of these spectra have a common feature, namely, bands at 3000–3650 cm^{-1} due to adsorbed water and hydroxyl groups. This property can be attributed to stretching vibrations of –OH in water. In particular, the adsorbed water content was significantly higher in the synthesized samples than in the TiO_2-P25 precursor due to the greater specific surface areas and pore volumes of the products. The band observed at 1630 cm^{-1} for all of the samples can be assigned to a water molecule bending mode [43]. Distinct broad bands in the 400–800 cm^{-1} region were assigned to Ti–O and Ti–O–Ti skeletal frequency regions [44]. Nearly every solvent used in this study has a low boiling point (under 100°C), facilitating its removal from crystals during calcination. These solvent characteristics may be the reason that FTIR spectra showed that nearly no organic components were present in these final products.

Figure 7 shows UV-vis absorption spectra of TiO_2 nanostructures. The band gaps of these samples were calculated from plots of $(\alpha h\nu)^2$ versus photon energy ($h\nu$) [45], Table 2. The results indicated that samples prepared in MEK and calcined at temperatures from 100 to 400°C and the W100 sample exhibited slight red shifts relative to pure TiO_2-P25. The estimated band gap energies were 3.20 eV for W100 and 3.21, 3.22, 3.20, and 3.22 eV for samples prepared in MEK calcined at 100, 200, 300, and 400°C, respectively, compared to pure TiO_2-P25 (3.25 eV). These band gap energies indicated that these samples were not phase mixtures but

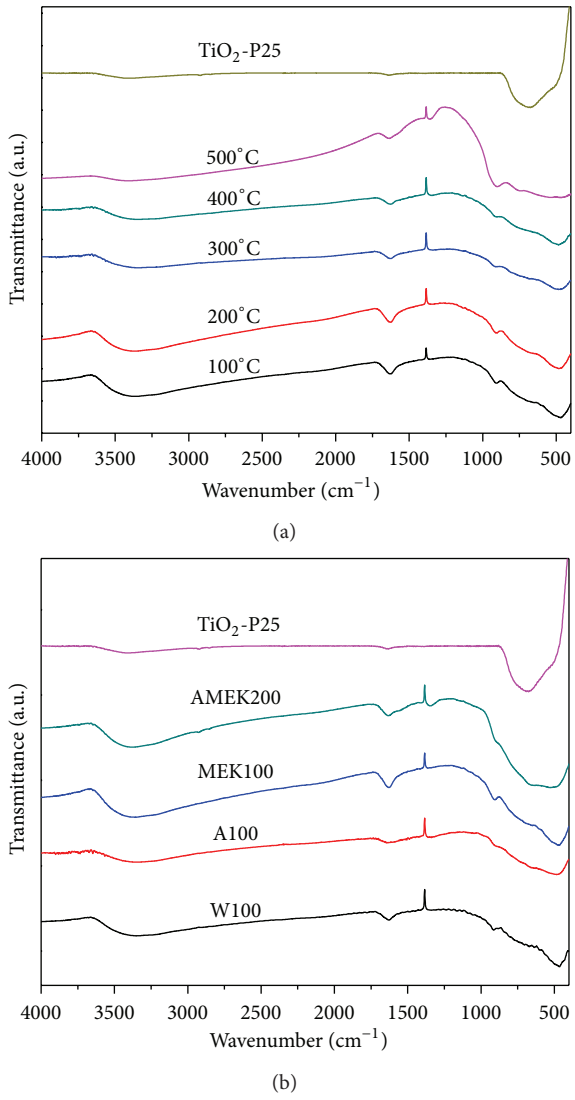

Figure 6: FTIR spectra. (a) Samples prepared using MEK and calcined at different temperatures, and (b) samples prepared using different solvents and calcined at different temperatures.

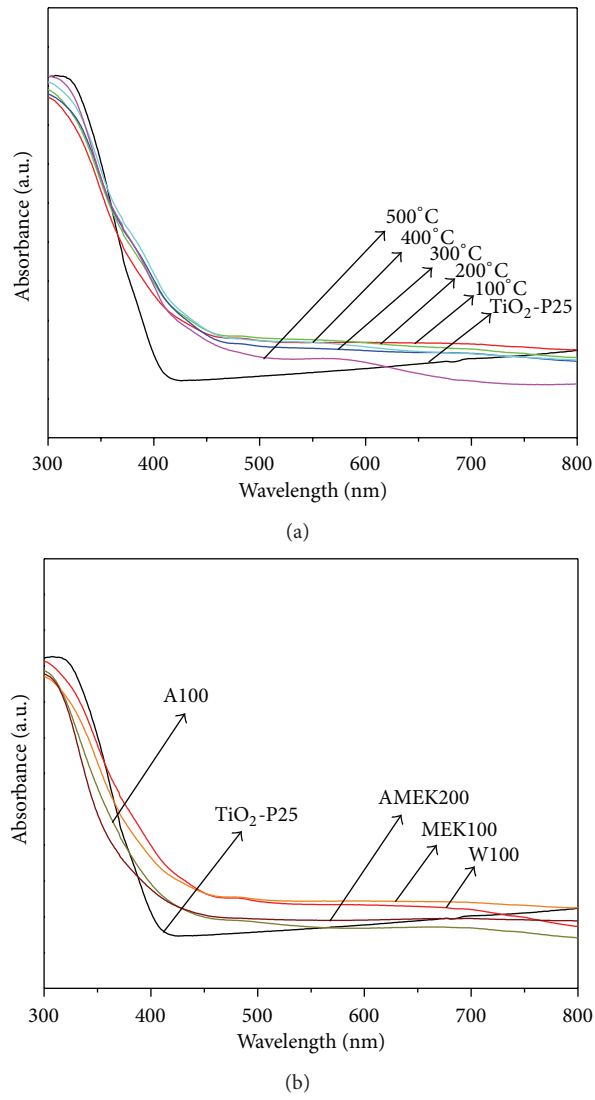

Figure 7: UV-vis absorbance spectra. (a) Samples prepared in MEK and calcined at different temperatures, and (b) samples prepared using various solvents and calcined at different temperatures.

rather contained only the titanate phase, shown by the XRD patterns and Raman spectra; these results are consistent with those for the phase compositions as shown in Table 2. In the mixed TiO_2/titanate phase, the titanate nanostructures normally have smaller band gaps than pure anatase TiO_2, and their band edges overlap, resulting in significant red shifts (reductions of band gap energies) [24, 46, 47]. The A100, AMEK200, and MEK500 samples exhibited blue shifts with estimated band gap energies of 3.36, 3.45, and 3.29 eV, respectively. These blue shifts were fully consistent with poor photocatalysis performance under visible-light irradiation by these samples (presented in the next section).

3.2. Photocatalytic Degradation of MB. In this experiment, the solution was stirred in darkness to reach adsorption equilibrium. The initial concentration of the dye solution (MB) after stirring was C_o. We selected samples prepared using MEK and different ketone solvents and calcined at various temperatures to carry out the photocatalytic reaction under visible light irradiation, Figure 8. The adsorption yield of MB solution in darkness and photodegradation efficiencies under visible light irradiation for all of the samples are listed in Table 3.

The results show that the sample prepared using MEK and calcined at 100°C was the most efficient photocatalyst, with MB removal equal to 77.3% after irradiation for 120 min. The MB photodegradation efficiency decreased when the calcination temperature increased (Figure 8(a)). The MEK100 sample also exhibited higher photodegradation efficiency than the W100 sample and TiO_2-P25 powder (Figure 8(b)). However, the W100 and MEK100 samples generally retained high adsorption efficiencies and were very efficient photocatalysts under visible light irradiation (Figure 8(b)). Given that samples W100 and MEK100 had better phase intensities

Table 3: Removal efficiency of MB in aqueous solution for different solvents.

Sample	Removal efficiency (adsorption) of MB solution in the dark for 60 min, %	Removal efficiency (photodegradation) of MB solution in visible light irradiation for 120 min, %	Overall removal efficiency of 180 min, %
Water (W)	Max at 100°C: 85.9	Max at 100°C: 72.7	Max at 100°C: 96.1
	Min at 500°C: 21.1	Min at 500°C: 13.5	Min at 500°C: 31.7
Acetone (Ac)	Max at 100°C: 38.7	Max at 100°C: 16.1	Max at 100°C: 48.6
	Min at 500°C: 21.1	Min at 500°C: 11.0	Min at 500°C: 29.9
Methyl ethyl ketone (MEK)	Max at 100°C: 85.0	Max at 100°C: 77.3	Max at 100°C: 96.6
	Min at 500°C: 18.2	Min at 500°C: 10.5	Min at 500°C: 26.8
Acetone : MEK (AMEK)	Max at 100°C: 42.6	Max at 200°C: 24.4	Max at 100°C: 55.9
	Min at 500°C: 16.6	Min at 500°C: 8.4	Min at 500°C: 23.6
TiO_2 precursor	12.9	11.6	23.0

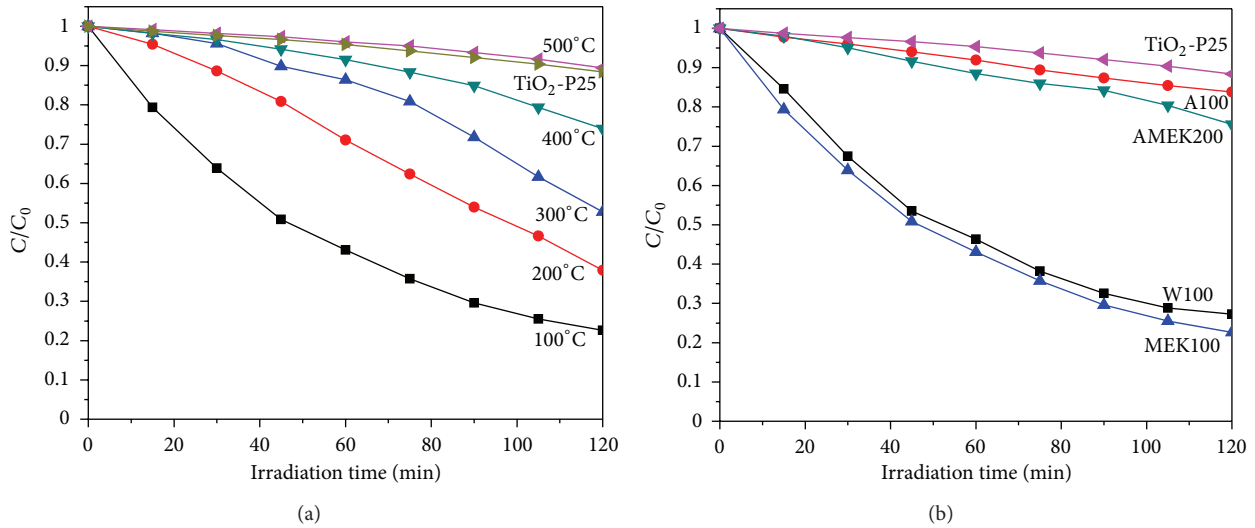

Figure 8: Photodegradation ratio of MB under visible light irradiation. (a) Samples prepared using MEK and calcined at temperatures from 100 to 500°C, and (b) samples using various solvents and calcined at different temperatures.

(in their XRD patterns and Raman spectra), their morphology consisted of nanotubes (TEM) with high specific surface areas (BET), and they exhibited better red shifts than other samples (UV-vis). Although the crystalline phase composition was mainly titanate (Table 2), sample MEK100 had a smaller crystallite size and lower average pore size (see Tables 1 and 2), the number of active surface sites and the surface charge carrier transfer rate increased. Therefore, the surface charge carrier transfer rate increased, and the photodegradation reaction was more efficient [48]. Increasing the calcination temperature produced an increase in the crystallite size (Table 2), a reduction in the specific area (Table 1), and a decrease in the photocatalytic efficiency (Figure 8(a)). Figure 8(b) also shows that samples A100 and AMEK200 had lower photocatalytic efficiencies after 120 min of visible light irradiation. This finding was entirely consistent with the above results for samples A100 and AMEK200, that is, less intense phases and blue shifts relative to TiO_2-P25 powder, with morphologies that were mainly nanoparticles or nanowires and with smaller specific surface areas.

The solubility, the diffusion process, and the chemical reactivity of the reactants are greatly enhanced [22] in solvothermal syntheses due to solvent properties, such as the density, the viscosity, and the diffusion coefficient, which can dramatically change product morphologies and sizes compared to conventional synthesis conditions [22, 49]. Thus, solvent selection is critical for controlling of chemical mechanisms leading to target materials. Reaction mechanisms induced during solvothermal reactions depend on physico-chemical solvent properties and can be indispensable for orienting the structural form of the product [25]. Every solvent used in this study had a low boiling point (below 100°C), such as acetone (56.5°C) and methyl ethyl ketone (79.6°C). The boiling point is an important solvent property because it determines the evaporation rate. When the synthesis temperature is 130°C, these solvents evaporate.

Acetone, in particular, has a low boiling point of 56.5°C, allowing for easier evaporation at its boiling point. Acetone can partially evaporate while mixing NaOH and sonicating TiO_2 powder because this reaction is highly exothermic. Evaporation may also affect the efficiency of creating TiO_2 nanotubes by solvothermal methods (although acetone is miscible in water) and indirectly reduce the adsorption and the photocatalysis efficiencies. The volatile nature of acetone may create adverse conditions for the solvothermal production of TiO_2 nanotubes, which can be seen in the TEM images of nanoparticle products. Although MEK has properties similar to those of acetone and is not completely miscible with water, it boils at a higher temperature and evaporates more slowly than acetone. These properties may enhance the efficiency of MEK for synthesizing TiO_2 nanotubes, and the products may have larger surface areas, Table 1. The photocatalytic reaction performance of TiO_2 products showed that samples prepared using MEK had higher efficiencies than samples prepared using water or acetone and that they were calcined at the same temperature (Figure 8(b)). The sample prepared using the mixed cosolvent of acetone and MEK had lower efficiency due to the effect of acetone, which diminished the performance of TiO_2, and the AMEK200 sample exhibited the best photocatalytic activity at 200°C (see Table 3). For Ac, AMEK, and MEK, adsorption in darkness, as well as the photocatalytic activity of the products prepared by the solvothermal method using ketone solvents, was in the following sequence: MEK > AMEK > Ac.

4. Conclusions

Various ketone solvents affected the morphology and the structure of TiO_2 products, as well as its photocatalytic degradation of MB dye. The samples prepared using MEK solvent and calcined at temperatures up to 400°C exhibited mainly titanate phases, but mixed phases of titanate (63.9%), anatase (19.1%), and rutile (17%) appeared at 500°C. Samples that were synthesized using solvents such as water and MEK were highly effective in adsorbing MB dye in darkness and photocatalytic reactions under visible light irradiation. The samples prepared in water and MEK were more efficient than their counterparts prepared in acetone or an acetone-MEK mixture and the TiO_2-P25 precursor because of their better phase intensities, nanotube morphologies, higher specific surface areas, and larger red shifts. The MEK100 sample exhibited the most efficient photodegradation of MB due to its smallest crystallite size. Generally, for most of the TiO_2 products prepared using different solvents, MB adsorption and photocatalytic efficiencies were the highest for samples calcined at 100°C and lowest at the calcination temperature of 500°C. However, for TiO_2 prepared using a cosolvent of acetone-MEK, the photocatalytic performance was the best for samples calcined at 200°C.

Acknowledgment

The authors wish to thank the National Science Council, NSC 99–2221-E-151-062, for their financial support of this study.

References

[1] A. Fujishima, T. N. Rao, and D. A. Tryk, "Titanium dioxide photocatalysis," *Journal of Photochemistry and Photobiology C*, vol. 1, no. 1, pp. 1–21, 2000.

[2] M. Kitano, M. Matsuoka, M. Ueshima, and M. Anpo, "Recent developments in titanium oxide-based photocatalysts," *Applied Catalysis A*, vol. 325, no. 1, pp. 1–14, 2007.

[3] T. Kasuga, M. Hiramatsu, A. Hoson, T. Sekino, and K. Niihara, "Titania nanotubes prepared by chemical processing," *Advanced Materials*, vol. 11, no. 15, pp. 1307–1311, 1999.

[4] C. C. Wang and J. Y. Ying, "Sol-gel synthesis and hydrothermal processing of anatase and rutile titania nanocrystals," *Chemistry of Materials*, vol. 11, no. 11, pp. 3113–3120, 1999.

[5] T. L. R. Hewer, E. C. C. Souza, T. S. Martins, E. N. S. Muccillo, and R. S. Freire, "Influence of neodymium ions on photocatalytic activity of TiO_2 synthesized by sol-gel and precipitation methods," *Journal of Molecular Catalysis A*, vol. 336, no. 1-2, pp. 58–63, 2011.

[6] X. Chen and S. S. Mao, "Titanium dioxide nanomaterials: synthesis, properties, modifications and applications," *Chemical Reviews*, vol. 107, no. 7, pp. 2891–2959, 2007.

[7] S. Sreekantan and L. C. Wei, "Study on the formation and photocatalytic activity of titanate nanotubes synthesized via hydrothermal method," *Journal of Alloys and Compounds*, vol. 490, no. 1-2, pp. 436–442, 2010.

[8] S. Mozia, E. Borowiak-Paleń, J. Przepiórski et al., "Physicochemical properties and possible photocatalytic applications of titanate nanotubes synthesized via hydrothermal method," *Journal of Physics and Chemistry of Solids*, vol. 71, no. 3, pp. 263–272, 2010.

[9] T. Kasuga, M. Hiramatsu, A. Hoson, T. Sekino, and K. Niihara, "Formation of titanium oxide nanotube," *Langmuir*, vol. 14, no. 12, pp. 3160–3163, 1998.

[10] G. H. Du, Q. Chen, R. C. Che, Z. Y. Yuan, and L. M. Peng, "Preparation and structure analysis of titanium oxide nanotubes," *Applied Physics Letters*, vol. 79, no. 22, pp. 3702–3705, 2001.

[11] B. D. Yao, Y. F. Chan, X. Y. Zhang, W. F. Zhang, Z. Y. Yang, and N. Wang, "Formation mechanism of TiO_2 nanotubes," *Applied Physics Letters*, vol. 82, no. 2, pp. 281–283, 2003.

[12] B. Poudel, W. Z. Wang, C. Dames et al., "Formation of crystallized titania nanotubes and their transformation into nanowires," *Nanotechnology*, vol. 16, no. 9, pp. 1935–1940, 2005.

[13] M. A. Khan, H. T. Jung, and O. B. Yang, "Synthesis and characterization of ultrahigh crystalline TiO_2 nanotubes," *Journal of Physical Chemistry B*, vol. 110, no. 13, pp. 6626–6630, 2006.

[14] R. Menzel, A. M. Peiró, J. R. Durrant, and M. S. P. Shaffer, "Impact of hydrothermal processing conditions on high aspect ratio titanate nanostructures," *Chemistry of Materials*, vol. 18, no. 25, pp. 6059–6068, 2006.

[15] J. Huang, Y. Cao, Q. Huang et al., "High-temperature formation of titanate nanotubes and the transformation mechanism of nanotubes into nanowires," *Crystal Growth and Design*, vol. 9, no. 8, pp. 3632–3637, 2009.

[16] D. V. Bavykin and F. C. Walsh, "Elongated titanate nanostructures and their applications," *European Journal of Inorganic Chemistry*, no. 8, pp. 977–997, 2009.

[17] M. Kang, S. Y. Lee, C. H. Chung et al., "Characterization of a TiO_2 photocatalyst synthesized by the solvothermal method

and its catalytic performance for $CHCl_3$ decomposition," *Journal of Photochemistry and Photobiology A*, vol. 144, no. 2-3, pp. 185–191, 2001.

[18] S. Yin, Y. Fujishiro, J. Wu, M. Aki, and T. Sato, "Synthesis and photocatalytic properties of fibrous titania by solvothermal reactions," *Journal of Materials Processing Technology*, vol. 137, no. 1–3, pp. 45–48, 2003.

[19] H. Kominami, J. I. Kato, S. Y. Murakami et al., "Solvothermal syntheses of semiconductor photocatalysts of ultra-high activities," *Catalysis Today*, vol. 84, no. 3-4, pp. 181–189, 2003.

[20] R. K. Wahi, Y. Liu, J. C. Falkner, and V. L. Colvin, "Solvothermal synthesis and characterization of anatase TiO_2 nanocrystals with ultrahigh surface area," *Journal of Colloid and Interface Science*, vol. 302, no. 2, pp. 530–536, 2006.

[21] R. C. Xie and J. K. Shang, "Morphological control in solvothermal synthesis of titanium oxide," *Journal of Materials Science*, vol. 42, no. 16, pp. 6583–6589, 2007.

[22] K. Das, S. K. Panda, and S. Chaudhuri, "Solvent-controlled synthesis of TiO_2 1D nanostructures: growth mechanism and characterization," *Journal of Crystal Growth*, vol. 310, no. 16, pp. 3792–3799, 2008.

[23] J. Yan, S. Feng, H. Lu et al., "Alcohol induced liquid-phase synthesis of rutile titania nanotubes," *Materials Science and Engineering B*, vol. 172, no. 2, pp. 114–120, 2010.

[24] B. Santara and P. K. Giri, "Impact of reaction temperature, stirring and cosolvent on the solvothermal synthesis of anatase TiO_2 and TiO_2/titanate hybrid nanostructures: elucidating the growth mechanism," *Materials Chemistry and Physics*, vol. 137, no. 3, pp. 928–936, 2013.

[25] G. Demazeau, "Solvothermal reactions: an original route for the synthesis of novel materials," *Journal of Materials Science*, vol. 43, no. 7, pp. 2104–2114, 2008.

[26] Q. R. Hu, S. L. Wang, P. Jiang, H. Xu, Y. Zhang, and W. H. Tang, "Synthesis of ZnO nanostructures in organic solvents and their photoluminescence properties," *Journal of Alloys and Compounds*, vol. 496, no. 1-2, pp. 494–499, 2010.

[27] K. Byrappa and T. Adschiri, "Hydrothermal technology for nanotechnology," *Progress in Crystal Growth and Characterization of Materials*, vol. 53, no. 2, pp. 117–166, 2007.

[28] S. Yin, Y. Aita, M. Komatsu, J. Wang, Q. Tang, and T. Sato, "Synthesis of excellent visible-light responsive $TiO_{2-X}N_y$ photocatalyst by a homogeneous precipitation- solvothermal process," *Journal of Materials Chemistry*, vol. 15, no. 6, pp. 674–682, 2005.

[29] U. Sulaeman, S. Yin, and T. Sato, "Solvothermal synthesis and photocatalytic properties of nitrogen-doped $SrTiO_3$ nanoparticles," *Journal of Nanomaterials*, vol. 2010, Article ID 629727, 6 pages, 2010.

[30] M. Kang, "Synthesis of Fe/TiO_2 photocatalyst with nanometer size by solvothermal method and the effect of H_2O addition on structural stability and photodecomposition of methanol," *Journal of Molecular Catalysis A*, vol. 197, no. 1-2, pp. 173–183, 2003.

[31] A. Sclafani, L. Palmisano, and M. Schiavello, "Influence of the preparation methods of TiO_2 on the photocatalytic degradation of phenol in aqueous dispersion," *Journal of Physical Chemistry*, vol. 94, no. 2, pp. 829–832, 1990.

[32] R. Ma, K. Fukuda, T. Sasaki, M. Osada, and Y. Bando, "Structural features of titanate nanotubes/nanobelts revealed by raman, X-ray absorption fine structure and electron diffraction characterizations," *Journal of Physical Chemistry B*, vol. 109, no. 13, pp. 6210–6214, 2005.

[33] A. Elsanousi, E. M. Elssfah, J. Zhang, J. Lin, H. S. Song, and C. Tang, "Hydrothermal treatment duration effect on the transformation of titanate nanotubes into nanoribbons," *Journal of Physical Chemistry C*, vol. 111, no. 39, pp. 14353–14357, 2007.

[34] D. L. Morgan, G. Triani, M. G. Blackford, N. A. Raftery, R. L. Frost, and E. R. Waclawik, "Alkaline hydrothermal kinetics in titanate nanostructure formation," *Journal of Materials Science*, vol. 46, no. 2, pp. 548–557, 2011.

[35] R. A. Zárate, S. Fuentes, J. P. Wiff, V. M. Fuenzalida, and A. L. Cabrera, "Chemical composition and phase identification of sodium titanate nanostructures grown from titania by hydrothermal processing," *Journal of Physics and Chemistry of Solids*, vol. 68, no. 4, pp. 628–637, 2007.

[36] R. A. Spurr and H. A. Myers, "Quantitative analysis of anatase-rutile mixtures with an X-ray diffractometer," *Analytical Chemistry*, vol. 29, no. 5, pp. 760–762, 1957.

[37] T. Ohsaka, F. Izumi, and Y. Fujiki, "Raman spectrum of anatase, TiO_2," *Journal of Raman Spectroscopy*, vol. 7, no. 6, pp. 321–324, 1978.

[38] T. Ohsaka, "Temperature dependence of the Raman spectrum in anatase TiO_2," *Journal of the Physical Society of Japan*, vol. 48, no. 5, pp. 1661–1668, 1980.

[39] G. A. Tompsett, G. A. Bowmaker, R. P. Cooney, J. B. Metson, K. A. Rogers, and J. M. Seakins, "The Raman spectrum of brookite, TiO_2 (*Pbca, Z* = 8)," *Journal of Raman Spectroscopy*, vol. 26, no. 1, pp. 57–62, 1995.

[40] B. L. Tian, Z. L. Du, Y. M. Ma et al., "Raman investigation of sodium titanate nanotubes under hydrostatic pressures up to 26.9 GPa," *Chinese Physics Letters*, vol. 27, no. 2, Article ID 026103, 2010.

[41] M. Nicol and M. Y. Fong, "Raman spectrum and polymorphism of titanium dioxide at high pressures," *Journal of Chemical Physics*, vol. 54, no. 7, pp. 3167–3170, 1971.

[42] F. Rojas, I. Kornhauser, C. Felipe et al., "Capillary condensation in heterogeneous mesoporous networks consisting of variable connectivity and pore-size correlation," *Physical Chemistry Chemical Physics*, vol. 4, no. 11, pp. 2346–2355, 2002.

[43] A. J. Maira, J. M. Coronado, V. Augugliaro, K. L. Yeung, J. C. Conesa, and J. Soria, "Fourier transform infrared study of the performance of nanostructured TiO_2 particles for the photocatalytic oxidation of gaseous toluene," *Journal of Catalysis*, vol. 202, no. 2, pp. 413–420, 2001.

[44] G. S. Guo, C. N. He, Z. H. Wang, F. B. Gu, and D. M. Han, "Synthesis of titania and titanate nanomaterials and their application in environmental analytical chemistry," *Talanta*, vol. 72, no. 5, pp. 1687–1692, 2007.

[45] H. Jia, Y. Hu, Y. Tang, and L. Zhang, "Synthesis and photoelectrochemical behavior of nanocrystalline CdS film electrodes," *Electrochemistry Communications*, vol. 8, no. 8, pp. 1381–1385, 2006.

[46] X. Sun and Y. Li, "Synthesis and characterization of ion-exchangeable titanate nanotubes," *Chemistry-A European Journal*, vol. 9, no. 10, pp. 2229–2238, 2003.

[47] H. Yu, J. Yu, B. Cheng, and M. Zhou, "Effects of hydrothermal post-treatment on microstructures and morphology of titanate nanoribbons," *Journal of Solid State Chemistry*, vol. 179, no. 2, pp. 349–354, 2006.

[48] R. Carrera-Lospez and S. Castillo-Cervantes, "Effect of the phase composition and crystallite size of sol-gel TiO_2 nanoparticles on the acetaldehyde photodecomposition," *Superficies y Vacio*, vol. 25, no. 2, pp. 82–87, 2012.

[49] G. Demazeau, "Solvothermal and hydrothermal processes: the main physico-chemical factors involved and new trends," *Research on Chemical Intermediates*, vol. 37, no. 2–5, pp. 107–123, 2011.